ACS APPLIED MATERIALS & INTERFACES

Research Article

www.acsami.org

Interrelationships among Grain Size, Surface Composition, Air Stability, and Interfacial Resistance of Al-Substituted $Li_7La_3Zr_2O_{12}$ Solid Electrolytes

Lei Cheng,[*,†,‡] Cheng Hao Wu,[§,∥] Angelique Jarry,[†] Wei Chen,[†] Yifan Ye,[⊥,#] Junfa Zhu,[#] Robert Kostecki,[†] Kristin Persson,[†] Jinghua Guo,[⊥] Miquel Salmeron,[‡,∥] Guoying Chen,[†] and Marca Doeff[*,†]

[†]Energy Storage and Distributed Resources Division, Lawrence Berkeley National Laboratory, Berkeley, California 94720, United States

[‡]Department of Material Sciences and Engineering, University of California, Berkeley, California 94720, United States

[§]Department of Chemistry, University of California, Berkeley, California 94720, United States

[∥]Material Science Division, Lawrence Berkeley National Laboratory, Berkeley, California 94720, United States

[⊥]Advanced Light Source, Lawrence Berkeley National Laboratory, University of California, Berkeley, California 94720, United States

[#]National Synchrotron Radiation Laboratory and Collaborative Innovation Center of Suzhou Nano Science and Technology, University of Science and Technology of China, Hefei 230029, P. R. China

Supporting Information

ABSTRACT: The interfacial resistances of symmetrical lithium cells containing Al-substituted $Li_7La_3Zr_2O_{12}$ (LLZO) solid electrolytes are sensitive to their microstructures and histories of exposure to air. Air exposure of LLZO samples with large grain sizes (~150 μm) results in dramatically increased interfacial impedances in cells containing them, compared to those with pristine large-grained samples. In contrast, a much smaller difference is seen between cells with small-grained (~20 μm) pristine and air-exposed LLZO samples. A combination of soft X-ray absorption (sXAS) and Raman spectroscopy, with probing depths ranging from nanometer to micrometer scales, revealed that the small-grained LLZO pellets are more air-stable than large-grained ones, forming far less surface Li_2CO_3 under both short- and long-term exposure conditions. Surface sensitive X-ray photoelectron spectroscopy (XPS) indicates that the better chemical stability of the small-grained LLZO is related to differences in the distribution of Al and Li at sample surfaces. Density functional theory calculations show that LLZO can react via two different pathways to form Li_2CO_3. The first, more rapid, pathway involves a reaction with moisture in air to form LiOH, which subsequently absorbs CO_2 to form Li_2CO_3. The second, slower, pathway involves direct reaction with CO_2 and is favored when surface lithium contents are lower, as with the small-grained samples. These observations have important implications for the operation of solid-state lithium batteries containing LLZO because the results suggest that the interfacial impedances of these devices is critically dependent upon specific characteristics of the solid electrolyte and how it is prepared.

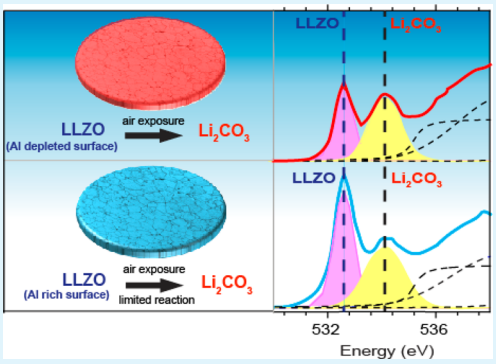

KEYWORDS: *interface, interfacial resistance, solid electrolyte, solid state battery, surface stability*

INTRODUCTION

One of the advantages of all solid-state rechargeable lithium batteries over conventional Li-ion configurations is the superior safety due to reduced risk of electrolytic solution leakage and the nonflammability of inorganic solid electrolytes. Moreover, the use of highly efficient solid packaging achieved by novel architectures both at the cell and stack levels results in less dead space, translating to improved energy density.[1] The critical scientific challenge in the development of all solid-state batteries centers on the solid electrolyte material, which must have high ionic conductivity, good chemical stability, and compatibility with electrode materials so that interfacial resistances are low. The selection of solid electrolyte candidate materials is quite limited by these stringent requirements. For example, highly conductive $Li_{1+x}Al_xTi_{2-x}(PO_4)_3$ (LATP),[2,3] and $Li_{10}GeP_2S_{12}$ (LGPS)[4] are hindered by instability against reduction by lithium metal,[5,6] and chemically stable phases such as LIPON[7] and Li_4SiO_4–Li_3PO_4[8,9] are handicapped by

Received: March 23, 2015
Accepted: July 20, 2015
Published: July 20, 2015

DOI: 10.1021/acsami.5b02528
ACS Appl. Mater. Interfaces 2015, 7, 17649–17655

low inherent ionic conductivity. In contrast, the highly conductive cubic phase $Li_7La_3Zr_2O_{12}$ (LLZO) emerges as a suitable candidate due to its chemical stability with respect to reduction versus lithium, and high ionic conductivity.[10−12] However, high resistances at Li/LLZO interfaces currently impede further development of this material, necessitating a more detailed understanding of the origin of the resistive interfaces.

One partially successful approach to decrease interfacial resistance is to apply external pressures as high as 150 MPa to improve the physical contacts between solid electrolyte and the lithium metal electrode.[13] However, such high pressure is not practical as it may lead to mechanical failure, especially with thin and brittle solid-state electrolytes. Another proposed strategy is to develop an ionically conductive coating to enhance the interfacial transport properties. This has met with some success in other solid electrolyte systems[14] but has not been reported for garnet solid electrolytes because of the lack of a candidate material that can integrate high ionic conductivity with superior chemical stability. Recently, Cheng et al. showed that the large resistance at Li/LLZO interfaces is not inherent to the material but originates from a small amount of Li_2CO_3 that forms on LLZO surfaces because of exposure to ambient air: a layer 10−100 nm thick can increase the interfacial resistance by an order of magnitude.[15] A polishing process in a protected environment, for example, Ar, can effectively remove the surface Li_2CO_3, which results in greatly improved interfacial properties. However, polishing in a protected environment is not practical or cost-effective for mass production. Thus, efforts to lower the interfacial resistance should be directed toward effective suppression of Li_2CO_3 formation upon brief air exposures that may occur during processing.

Herein, we reveal the interrelationships between grain-size, surface composition, surface−air stability, and interfacial resistances of LLZO solid electrolytes. Specifically, we report that the chemical tolerance of LLZO pellets toward exposure to ambient air is intimately related to the microstructure because of differences in grain and grain boundary chemistries. The formation of surface Li_2CO_3 is much less for samples with small grains compared to those with large grains, even after air exposure, leading to decreased interfacial impedances in symmetrical cells with lithium electrodes. This obviates the need for polishing and simplifies the processing of LLZO materials into forms appropriate for use in electrochemical devices, bringing garnet solid electrolytes a step further toward practical application in solid state batteries.

EXPERIMENTAL SECTION

LLZO pristine powders were prepared using a solid-state reaction as reported in our previous work,[16] using the following precursors: Li_2CO_3 (CAS# 554-13-2 Aldrich >99.0%), Al_2O_3 (Alcoa), ZrO_2 (CAS# 1314-23-4 Aldrich 99%), and $La(OH)_3$ (CAS# 14507-19-8 Alfa 99.95% REO). The as-prepared fresh powder was ground and then attrition milled at 450 rpm for 2 h with 2 mm diameter ZrO_2 media in isopropyl alcohol (IPA). The attrition-milled powder was used as-is for the large-grained samples. Unmilled powder (10 wt %) was mixed with 90 wt % attrition-milled powder to make small-grained samples (see ref 17). Pellets were made by cold uniaxial pressing using a 3/8 in. stainless die without binder. Dense large- and small-grained LLZO pellets were both pressed and sintered at 1100 °C for 12 h, following procedures reported in ref 17. Typical dimensions of the pellets were around 1.1 mm thick and 7.8 mm in diameter. Pellets designated P_LLZO_S and P_LLZO_L (see Table 1) were polished using 400 and 600 grit number polishing paper in an Ar-filled Vacuum Atmospheres Nexus II glovebox equipped with an inert gas purifier, with O_2 and moisture levels below 1 ppm. After the polishing procedure, some of the pellets were transferred out of glovebox to expose them to air for different periods of time. ICP-OES measurements of P_LLZO_L and P_LLZO_S were carried out by the Evans Analytical Group. Surface images of the LLZO pellets were obtained by scanning electron microscopy (SEM) using a JEOL-7500F field emission microscope or a HITACHI TM-1000 tabletop microscope, using secondary electron imaging (SEI) mode.

Table 1. Sample Labeling and Processing Histories

sample label	exposure	grain size (μm)	exposure time
P_LLZO_L	pristine	150−200	n/a
E_LLZO_L24h	exposed	150−200	24 h
E_LLZO_L6m	exposed	150−200	6 months
P_LLZO_S	pristine	20	n/a
E_LLZO_S24h	exposed	20	24 h
E_LLZO_S6m	exposed	20	6 months

AC impedance measurements were obtained on the dense pellets using a VMP3 multichannel potentiostat/galvanostat (Bio-Logic Science Instruments) equipped with frequency response analyzers. Soft metallic lithium was first spread on both sides of the dense pellet. Afterward, the pellet was assembled in a Swagelok-type cell between lithium foil disks on both sides. Physical contacts were maintained by compression of the spring at controlled displacement in the Swagelok cell with an estimated pressure of 200 kPa, derived from considering the spring displacement and spring constant. Samples were assembled in the same Swagelok cell with controlled displacement so that similar pressures were used for each. Impedance data were collected at frequencies from 1 MHz to 1 Hz. Several samples were examined by impedance analysis and representative results are presented in this paper.

O K-edge soft X-ray absorption spectroscopy (sXAS) experiments were performed at undulator beamline 8.0.1 at the Advanced Light Source, Lawrence Berkeley National Laboratory. The intense photon beam from a spherical grating monochromator gives an energy resolution better than 0.2 eV. Spectra were collected using both surface-sensitive total electron yield (TEY) and bulk-sensitive total fluorescence yield (TFY) at ambient temperature. All the spectra have been normalized to the beam flux measured by the upstream gold mesh.

Raman spectra of the pellets were recorded on a "Labram" Raman confocal microscope system (ISA Groupe Horiba) in the confocal backscattering configuration with a 488 nm Argon ion laser (Coherent Inc. Innova 70), a plan olympus 10× magnification, a 0.25 numerical aperture objective lense and a 22 focal length. The beam intensity was adjusted to 0.1 mW for a beam diameter of 2 μm.

XPS studies of the polished LLZO pellets were performed using a PHI 5400 XPS system equipped with an Al X-ray source (incident photon energy of 1486.7 eV). XPS samples were sealed in a sample transfer tool under Ar environment. The aperture size was set to 1.1 mm in diameter. The binding energy of the obtained XPS spectra was calibrated with respect to the C 1s peak of adventitious carbon at 284.8 eV. XPS spectra were quantitatively analyzed by deconvoluting Voigt-type line-shapes, preceded by subtracting Shirley-type background (for Zr 3d spectra) and linear background (for Al 2p and Li 1s spectra).

COMPUTATIONAL SECTION

First-principles total energy calculations were carried out using density functional theory and the projector augmented-wave (PAW) approach as implemented in the Vienna ab initio simulation package (VASP).[18−20] The generalized gradient approximation (GGA) of Perdew−Burke−Ernzerhof (PBE) was used to approximate the electronic change and correlation.[21] The structures for the original LLZO and Al-substituted LLZO were taken from the Inorganic Crystal Structure Database (ICSD) (Collection codes 422259 and 185539).[22,23] The Li and Al atoms were ordered in a supercell using the Python Materials Genomics (pymatgen) code with experimental

DOI: 10.1021/acsami.5b02528
ACS Appl. Mater. Interfaces 2015, 7, 17649−17655

site occupancies reported from ICSD. All configurations were enumerated so that 2 Li atoms and 1 O atom were removed from the starting LLZO structure. The lowest electrostatic energy configuration was chosen for the LLZO structure after reaction (denoted as $Li_{54}La_{24}Zr_{16}O_{95}$). These structures were fully relaxed to converge the final energy within 5 meV per formula unit. The plane wave energy cutoff was 520 eV and the Brillouin-zone was sampled at the Γ-point.

The total energies for Li_2O, Li_2CO_3, and LiOH were taken from the Materials Project (https://www.materialsproject.org/). These calculations were performed using a compatible set of parameters with the calculations in the current study.[21] The calculated formation enthalpies for all compounds were referenced using a thermodynamic framework that corrects the DFT errors in gases and aqueous states, allowing extrapolation to room temperature from 0 K.[24] We used the experimental Gibbs free energies for the gas phase H_2O and CO_2 in following thermodynamic calculations.

RESULTS AND DISCUSSION

We have previously reported details of the fabrication of small- and large-grained dense Al-substituted LLZO pellets.[17] Figure 1

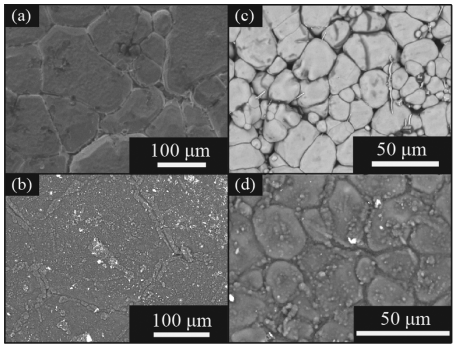

Figure 1. Top view SEM images of (a) as-sintered large-grained LLZO, (b) large-grained LLZO after 6 month exposure to ambient air, (c) as-sintered small-grained LLZO, and (d) small-grained LLZO after 6 months exposure to ambient air.

shows the scanning electron microscopy (SEM) images of the surface morphologies of as-sintered samples with different grain sizes, as well as those aged for six months in an ambient air environment. It is clear that the surfaces changed after the extended period of air exposure. Both small- and large-grained LLZO pellets show evidence of reaction layers, which obscured the grain and grain boundary features, preventing clear imaging. The phenomenon of surface morphology change is very similar to what Jin and McGinn observed: a reaction layer forms on garnet electrolyte after 1 week of air exposure.[25]

To evaluate the impact of air exposure on the interfacial resistances, small- and large-grained LLZO pellets were both carefully polished in an Ar atmosphere to minimize variations in surface roughness. These samples are designated P_LLZO_S and P_LLZO_L for small- and large-grained pellets, respectively. Some of the polished pellets were transferred out of the glovebox and stored in air for either 24 h or 6 months. These air-exposed small- and large-grained LLZO pellets are designated E_LLZO_S24h, E_LLZO_L24h and E_LLZO_S6m, E_LLZO_L6m (Table 1). The resistances of LLZO/Li interfaces were determined by AC-impedance. Measurements were carried out on symmetrical cells containing pristine LLZO samples and those exposed to air for 24 h and 6 months, sandwiched between nonblocking lithium electrodes. The Nyquist plots, equivalent circuits, and results of the fittings are provided in Figure 2 and Table 2. A partial semicircle in the high frequency range and a complete semicircle in the lower frequency range were observed in Nyquist plots for both the pristine samples and the air-exposed samples. The semicircles at higher frequency ranges were attributed to total resistances of pellets (R_{pellet}), and lower frequency ones to interfacial resistances ($R_{interface}$). The area specific interfacial resistances (ASRs) were then determined using the low frequency semicircles, following the procedures described in refs 9, 15, and 17. The ASRs determined for cells containing the pristine and air-exposed samples are also plotted in Figure 2c for comparison. This shows that there was a nearly 1 order of magnitude increase in the ASR, from 103 to 880 Ω cm^2 for the large-grained sample after 24 h of exposure to air. In contrast, the increase for the small-grained sample was much slighter; 64 Ω cm^2 measured for 24 h exposure sample E_LLZO_S24h compared to 38 Ω cm^2 for the unexposed pristine sample. The impedance data for symmetrical cells containing 6-month exposure samples of E_LLZO_L6m and E_LLZO_S6m are provided in Figure S1. These Nyquist plots are similar to those previously reported for cells containing exposed samples,[23,26] and show a considerable increase in the total impedance compared to the pristine samples and those exposed to air for 24 h. Nevertheless, small-grained E_LLZO_S6m is markedly less resistive than E_LLZO_L6m. These data suggest that the

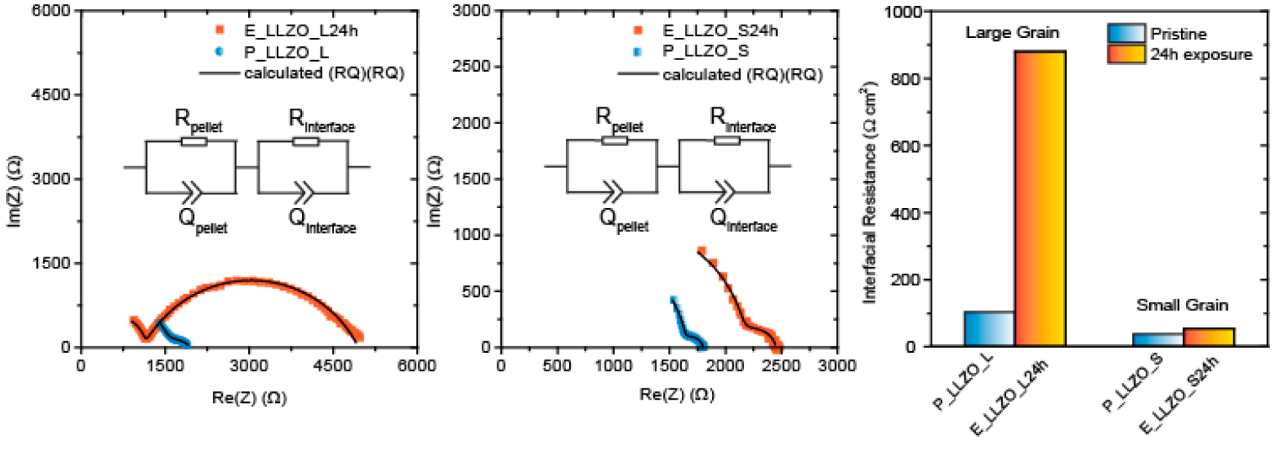

Figure 2. Nyquist plots of impedance data of Li/LLZO/Li cells containing: (a) P_LLZO_L and E_LLZO_L24h and (b) P_LLZO_S and E_LLZO_S24h. (c) Area specific interfacial resistances (ASRs) of pristine LLZO samples and those exposed to air for 24 h.

DOI: 10.1021/acsami.5b02528
ACS Appl. Mater. Interfaces 2015, 7, 17649−17655

Table 2. Results from EIS Fitting of Li/LLZO/Li Symmetrical Cells

sample	R_{pellet} (Ω)	Q_{pellet} (10^{-12} F)	$R_{interface}$ (Ω)	$Q_{interface}$ (10^{-6} F)	χ^2	interfacial resistance (Ω cm^2)
P_LLZO_S	1635	65.15	164	0.16	1.674×10^{-3}	38
E_LLZO_S24h	2174	83.80	278	0.13	2.238×10^{-3}	64
P_LLZO_L	1495	141.30	446	1.9	0.519×10^{-3}	103
E_LLZO_L24h	1114	111.60	3835	0.85	7.623×10^{-3}	880

small-grained LLZO samples are more air-stable than the large-grained ones. We speculated that less Li_2CO_3 is formed on the small-grained sample than the large-grained one during comparable periods of air exposure, since Li_2CO_3 on the LLZO surface is closely linked with a rise in interfacial resistance.[15]

To investigate details of the Li_2CO_3 formation and how microstructure affects it, several techniques were used to probe various sample depths. To qualitatively estimate the Li_2CO_3 content formed on both E_LLZO_S24h and E_LLZO_L24h surfaces after a short period of air exposure, soft X-ray absorption spectroscopy (sXAS) was employed. The spot size of the X-ray is approximately 1.5 mm for these experiments. In surface sensitive total electron yield mode (TEY), approximately a 10 nm depth near the surface is measured for this experimental setup and sample type, whereas in total fluorescence yield mode (TFY) ≈ 100 nm is probed. Figure 3 shows the normalized O K-edge spectra of the unexposed

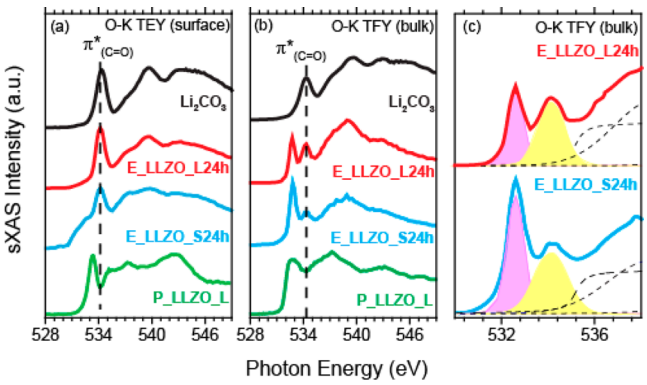

Figure 3. (a and b) Normalized O K-edge XAS spectra of P_LLZO_L reference (bottom), air-exposed E_LLZO_S24h (second from bottom), E_LLZO_L24h (second from top), and Li_2CO_3 reference (top) collected in TEY and TFY modes. (c) Expanded region of the O K-edge spectra of E_LLZO_L24h and E_LLZO_S24h samples with fitted LLZO and Li_2CO_3 peaks.

LLZO reference (P_LLZO_L, pristine LLZO), Li_2CO_3 reference, E_LLZO_L24h (large grained sample after 24 h air exposure), and E_LLZO_S24h (small grained sample after 24 h air exposure), collected in both TEY and TFY modes. The Li_2CO_3 reference has a major absorption peak at 534 eV, which is assigned to the O 1s to π^* (C═O) transition.[27] The leading edge of the LLZO reference is located at a lower energy of 533 eV. In the surface sensitive TEY mode, the E_LLZO_L24h spectrum resembles that of the Li_2CO_3 reference, suggesting that the sample was completely covered by Li_2CO_3 to a depth of several nanometers. The spectrum of the E_LLZO_S24h sample is slightly different: although a strong peak due to Li_2CO_3 is also observed, the broad shoulder peak at 533 eV is still evident, indicating less complete coverage of the surface with Li_2CO_3 than in the case of the large-grained sample. The TFY mode, which probes more deeply, was also used to compare the samples. Both show clear absorption features of LLZO and Li_2CO_3 at 533 and 534 eV respectively, suggesting that the coverage of Li_2CO_3 is less than 100 nm deep in both cases. A very intense LLZO peak is observed in the spectrum of the exposed E_LLZO_S24h sample, which also has a relatively weak Li_2CO_3 feature, while in the spectrum of E_LLZO_L24h, the two peaks have similar intensities. Extra details can be extracted from the peak deconvolution in the expanded region of the TFY O K-edge spectra, shown in Figure 1c. The Li_2CO_3 to LLZO peak area ratio in the spectrum of E-LLZO_S24h is 0.96, while that for the LLZO_LG spectrum is 1.33, a higher value. Thus, the TFY O K-edge spectra confirm that the E_LLZO_S24h (small grained sample after 24 h air exposure) surface is covered with less Li_2CO_3 than the E_LLZO_L24h (large grained sample after 24 h air exposure) one. This, in turn, suggested lower air reactivity for the small-grained sample compared to the large-grained one, in good agreement with impedance data.

In the case of the samples exposed to air for six months, sXAS experiments are not likely to be informative, as the thickness of the Li_2CO_3 layer may exceed the maximum probing depth. Laser-induced breakdown spectroscopy (LIBS)[15,16] experiments have previously shown that the Li_2CO_3 layer is ∼1 μm deep on LLZO pellet surfaces after several months exposure time. Raman spectroscopy, on the other hand, is particularly suitable for probing these species at this length scale. In Raman spectroscopy, the peak intensity related to different species can be used for comparative analysis.[28] Figure 4 shows typical Raman spectra of the

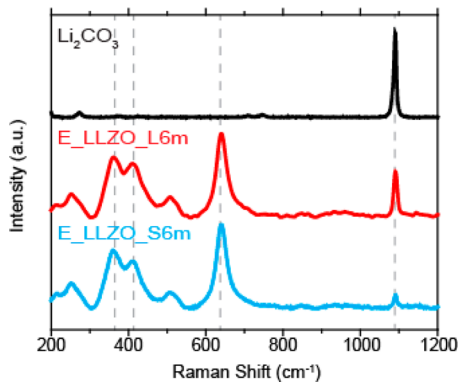

Figure 4. Typical Raman spectra of E_LLZO_S6m (bottom), E_LLZO_L6m (middle), and Li_2CO_3 reference (top). LLZO Spectra were normalized to the peak at 640 cm^{-1}.

E_LLZO_S6m (small grained sample after 6 month air exposure) and E_LLZO_L6m (large grained sample after 6 month air exposure) pellets and a Li_2CO_3 reference.[29] The LLZO spectra are in agreement with the literature and previous reports,[30] with the strongest peak at 640 cm^{-1} assigned to vibrational stretching modes of ZrO_6 octahedral units and the peak at ∼1100 cm^{-1} assigned to Li_2CO_3.[30−32] To correct for crystal orientation effects, as well as heterogeneities in coverage,

DOI: 10.1021/acsami.5b02528
ACS Appl. Mater. Interfaces 2015, 7, 17649−17655

Raman spectra were collected at 15 different locations on each sample and normalized to the LLZO peak at 640 cm^{-1}. The averaged relative peak area ratios of Li_2CO_3 to LLZO are presented in Table S1. A 9.3% ± 2.4% peak intensity ratio was determined for E_LLZO_L6m (large-grained sample exposed to air for six months) and a value about two times lower (4.9% ± 1.2%) for E_LLZO_S6m (small-grained sample exposed to air for six months), clearly confirming that less Li_2CO_3 is formed on the E_LLZO_S6m surface compared to the E_LLZO_L6m surface after 6 months of air exposure.

Evidence from the sXAS and Raman spectroscopy experiments together confirmed that the amount of Li_2CO_3 formed during air exposure differs depending on the grain size of the LLZO samples. This suggests that there may be differences in the surface chemistries of the two types of samples, presuming that the formation of Li_2CO_3 can only be initiated on clean dense LLZO surfaces when a carbon source (CO_2) is present and in contact. We used surface-sensitive XPS to study the surface compositions of pristine P_LLZO_L and P_LLZO_S samples to obtain more information. The X-ray beam size for these experiments is about 1.1 × 1.1 mm in area, similar to the beam footprint of sXAS. The probing depth of the XPS is estimated to be 2−3 nm considering the electron inelastic mean-free path in inorganic materials.[33] The Zr 3d, Li 1s, and Al 2p XPS spectra of the pristine samples are provided in Figure 5 (intensities normalized to Zr 3d). No Al signal was

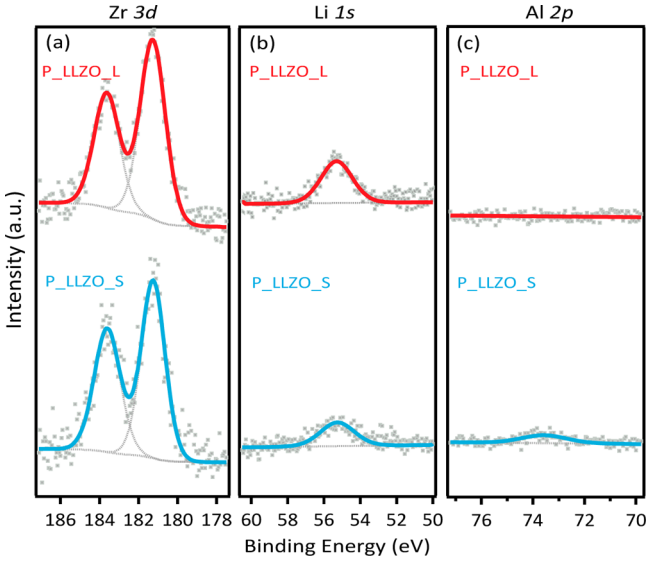

Figure 5. (a) Zr 3d, (b) Li 1s, aand (c) Al 2p XPS spectra of P_LLZO_L (top) and P_LLZO_S (bottom).

identified in P_LLZO_L but is clearly discernible in P_LLZO_S in spite of the low Al concentration and the fact that the bulk compositions of these pellets are nearly identical (see Table S2). In the crystal structure, Al ions substitute at Li sites, each one replacing three Li^+ ions for charge neutrality in the Al-substituted cubic phase LLZO. NMR and computational studies indicate that Al is located both at 24d and 96h sites, but the 24d site is energetically preferred.[11,34] The Li 1s, Al 2p, and Zr 3d XPS peak areas were compared and tabulated in Table S3, confirming that the P_LLZO_S has a lower Li/Zr ratio and higher Al/Zr ratio compared to P_LLZO_L. The semi-quantitative comparisons of the Li 1s spectra also show that the surface of P_LLZO_L contains more Li than that of P_LLZO_S. These results may be explained by differences in the sintering behaviors between the large-grained and small-grained samples. In P_LLZO_L, a liquid sintering mechanism appears to be actively involved, resulting in Al rich "pockets" that segregate from the lattice and accumulate between grains inside the pellets.[16,35] This phenomenon has been observed by several groups, including ours, and is processing-condition dependent.[36−38] The segregates deplete the Al in the lattice resulting in diminished Al intensity in the XPS experiments, because the Al-rich pockets are buried within the pellet and inaccessible to XPS. EDS analysis (Figure S2) also shows much greater Al compositional variation for the large-grained sample compared to the small-grained one, although the overall Al/Zr ratio was lower on average for the former. The small-grained LLZO appears to sinter by a different mechanism, which limits grain growth and does not leads to as much Al enrichment at grain boundaries.[17] Higher Al and lower Li contents at sample surfaces result in less Li_2CO_3 formation upon air exposure, as well as lower interfacial resistances. This insight agrees well with experimental observations made by Buschmann et al.[39] that cells containing garnet $Li_{5.756}Al_{0.29}La_3Zr_{1.625}Ta_{0.375}O_{12}$ have lower interfacial resistances compared to either $Li_6La_3ZrTaO_{12}$ or $Li_{6.16}Al_{0.28}La_3Zr_2O_{12}$, both of which have higher lithium and lower Al contents.

To elucidate why the surface chemical composition of the garnet structure is critical for determining tolerance against formation of Li_2CO_3 during air exposure, first-principles calculations based on density functional theory were performed to evaluate the thermodynamic tendency of LLZO to form Li_2CO_3 with possible reactants present in air. We considered the following chemical reactions of Al-substituted and Al-free LLZO.

$$Li_{56}La_{24}Zr_{16}O_{96}\ (s) + H_2O\ (g) = Li_{54}La_{24}Zr_{16}O_{95}\ (s) + 2LiOH\ (s) \quad (1)$$

$$Li_{56}La_{24}Zr_{16}O_{96}\ (s) + CO_2\ (g) = Li_{54}La_{24}Zr_{16}O_{95}\ (s) + Li_2CO_3 \quad (2)$$

$$Li_{50}Al_2La_{24}Zr_{16}O_{96}\ (s) + H_2O\ (g) = Li_{48}Al_2La_{24}Zr_{16}O_{95}\ (s) + 2LiOH \quad (3)$$

$$Li_{50}Al_2La_{24}Zr_{16}O_{96}\ (s) + CO_2\ (g) = Li_{48}Al_2La_{24}Zr_{16}O_{95}\ (s) + Li_2CO_3 \quad (4)$$

The formation of LiOH or Li_2CO_3 from these reactions is accompanied by the loss of Li in LLZO and presumably compensated by concurrent O loss to balance the charge, resulting in $Li_{54}La_{24}Zr_{16}O_{95}$.[15] In fact, Jin et al. reported that garnet reacts with water to form LiOH[25] and Wang et al. observed a reaction with dry CO_2.[40] The Gibbs free energies of all related chemical species are tabulated in Table S4 and for reactions 1−4 in Table 3. Comparison of the reaction Gibbs free energies indicates that for both Al-free and Al-substituted LLZO, the reactions 2 and 4 with gas phase CO_2 are energetically favorable, consistent with the experimental observations of Li_2CO_3 on the surfaces of both samples of Al-substituted LLZO in this study. However, the thermodynamic tendencies for the reactions with gas phase H_2O (1 and 3) are very different. The reaction of unsubstituted LLZO with moisture is possible with a Gibbs free energy of −0.53 eV. In

DOI: 10.1021/acsami.5b02528
ACS Appl. Mater. Interfaces 2015, 7, 17649−17655

Table 3. Gibbs Free Energy of Possible Chemical Reactions

chemical reaction	Gibbs energy (eV)
$Li_{56}La_{24}Zr_{16}O_{96}$ (s) + H_2O (g) = $Li_{54}La_{24}Zr_{16}O_{95}$ (s) + 2LiOH (s)	−0.53
$Li_{56}La_{24}Zr_{16}O_{96}$ (s) +CO_2 (g) = $Li_{54}La_{24}Zr_{16}O_{95}$ (s) + Li_2CO_3 (s)	−1.99
$Li_{50}Al_2La_{24}Zr_{16}O_{96}$ (s) + H_2O (g) = $Li_{48}Al_2La_{24}Zr_{16}O_{95}$ (s) + 2LiOH (s)	0.42
$Li_{50}Al_2La_{24}Zr_{16}O_{96}$ (s) + CO_2 (g) = $Li_{48}Al_2La_{24}Zr_{16}O_{95}$ (s) + Li_2CO_3 (s)	−1.04

contrast, the reaction of Al substituted LLZO with moisture reaction 3 is not energetically favored because it has a positive Gibbs energy of 0.42 eV. LiOH is known to be a good CO_2 absorber,[41] so that Li_2CO_3 is subsequently formed after the reaction with moisture occurs. The formation of Li_2CO_3 via direct reaction with CO_2 eqs 1 and 2 is likely to be kinetically slower than formation of LiOH by reaction 3, as it involves one more lithium than LiOH. The fact that LiOH is not predicted to form readily when Al-substituted LLZO is exposed to moist air limits production of Li_2CO_3 to the slower route of direct reaction with CO_2 in air. The substitution of Al for Li sites limits Li ion motion,[42] disrupting Li pathways through 24d−48g−24d sites, resulting in lower reactivity. This is further supported by the observation that Al-free cubic LLZO has better conductivity than Al-substituted counterparts.[37]

CONCLUSIONS

X-ray absorption and Raman spectroscopy with different probing depths were used to determine the extent of Li_2CO_3 formation on LLZO pellets having different microstructures after air exposure. Small-grained samples formed less Li_2CO_3 on surfaces after both short and long-term ambient air exposures, compared to large-grained samples. The extent of formation of Li_2CO_3 on LLZO pellet surfaces correlates well with area specific resistances measured by impedance experiments on symmetrical cells with lithium electrodes containing the solid electrolyte samples; a much more dramatic rise in impedance after exposure to air for 24 h is seen for the large-grained samples than for the small-grained ones. The differences in behavior are attributed to variations in the bulk compositions due to dissimilar sintering mechanisms for the two types of samples. In large-grained samples, Al segregates at grain boundaries resulting in depletion from the bulk, while Al is retained in the grains of the small-grained samples. DFT calculations indicate that Al-substituted LLZO is less likely to react with water present in air to form LiOH, with subsequent conversion to Li_2CO_3 upon reaction with CO_2, than its unsubstituted analog. Although both materials can also react directly with CO_2 in air, this route for formation of Li_2CO_3 is expected to be much slower than that involving water. These results indicate that variations in microstructures lead to differing surface compositions and are critical for improved air stability and low interfacial resistances in devices containing these electrolytes.

ASSOCIATED CONTENT

Supporting Information

The Supporting Information is available free of charge on the ACS Publications website at DOI: 10.1021/acsami.5b02528.

Nyquist plots, ICP element analysis, EDS line scans, XPS data, and DFT calculations (PDF)

AUTHOR INFORMATION

Corresponding Authors

*E-mail: leicheng@lbl.gov.
*E-mail: mmdoeff@lbl.gov.

Notes

This document was prepared as an account of work sponsored by the United States Government. While this document is believed to contain correct information, neither the United States Government nor any agency thereof, nor the Regents of the University of California, nor any of their employees, makes any warranty, express or implied, or assumes any legal responsibility for the accuracy, completeness, or usefulness of any information, apparatus, product, or process disclosed, or represents that its use would not infringe privately owned rights. Reference herein to any specific commercial product, process, or service by its trade name, trademark, manufacturer, or otherwise, does not necessarily constitute or imply its endorsement, recommendation, or favoring by the United States Government or any agency thereof, or the Regents of the University of California. The views and opinions of authors expressed herein do not necessarily state or reflect those of the United States Government or any agency thereof or the Regents of the University of California.
The authors declare no competing financial interest.

ACKNOWLEDGMENTS

This work was supported by the Assistant Secretary for Energy Efficiency and Renewable Energy, Office of Vehicle Technologies and the Chemical Sciences, Geosciences, and Biosciences Division, Office of Basic Energy Sciences of the U.S. Department of Energy under contract no. DE-AC02-05CH11231. The Advanced Light Source is supported by the Director Office of Science, Office of Basic Energy Sciences, of the U.S. Department of Energy under Contract No. DE-AC02-05CH11231. L.C., G.C, and M.D acknowledge illuminating discussions with Dr. Thomas Richardson. Prof. Lutgard De Jonghe is cordially acknowledged for the discussion on solid electrolytes. L.C. would like to acknowledge Mr. James Wu and Mr. Yuyi Li for assistance with instruments and Dr. Wanli Yang and Dr. Ruimin Qiao for helpful discussion on soft X-ray spectroscopy. W.C. gratefully acknowledges the Materials Project Center (BES DOE Grant No. EDCBEE) for funding support. C.H.W. acknowledges the Advanced Light Source Doctoral Fellowship in Residence.

REFERENCES

(1) Takada, K. Progress and Prospective of Solid-State Lithium Batteries. *Acta Mater.* **2013**, *61*, 759−770.
(2) Aono, H. Ionic Conductivity of Solid Electrolytes Based on Lithium Titanium Phosphate. *J. Electrochem. Soc.* **1990**, *137*, 1023−1027.
(3) Knauth, P. Inorganic Solid Li Ion Conductors: An Overview. *Solid State Ionics* **2009**, *180*, 911−916.
(4) Kamaya, N.; Homma, K.; Yamakawa, Y.; Hirayama, M.; Kanno, R.; Yonemura, M.; Kamiyama, T.; Kato, Y.; Hama, S.; Kawamoto, K.; Mitsui, A. A Lithium Superionic Conductor. *Nat. Mater.* **2011**, *10*, 682−686.
(5) Hartmann, P.; Leichtweiss, T.; Busche, M. R.; Schneider, M.; Reich, M.; Sann, J.; Adelhelm, P.; Janek, J. Degradation of NASICON-Type Materials in Contact with Lithium Metal: Formation of Mixed Conducting Interphases (MCI) on Solid Electrolytes. *J. Phys. Chem. C* **2013**, *117*, 21064−21074.
(6) Ong, S. P.; Mo, Y.; Richards, W. D.; Miara, L.; Lee, H. S.; Ceder, G. Phase Stability, Electrochemical Stability and Ionic Conductivity of

DOI: 10.1021/acsami.5b02528
ACS Appl. Mater. Interfaces 2015, 7, 17649−17655

the $Li_{10\pm1}MP_2X_{12}$ (M = Ge, Si, Sn, Al or P, and X = O, S or Se) Family of Superionic Conductors. *Energy Environ. Sci.* **2013**, *6*, 148−156.
(7) Bates, J. Electrical Properties of Amorphous Lithium Electrolyte Thin Films. *Solid State Ionics* **1992**, *53*−*56*, 647−654.
(8) Hu, Y.-W. Ionic Conductivity of Lithium Orthosilicate—Lithium Phosphate Solid Solutions. *J. Electrochem. Soc.* **1977**, *124*, 1240−1242.
(9) Zhang, L.; Cheng, L.; Cabana, J.; Chen, G.; Doeff, M. M.; Richardson, T. J. Effect of Lithium Borate Addition on the Physical and Electrochemical Properties of the Lithium Ion Conductor $Li_{3.4}Si_{0.4}P_{0.6}O_4$. *Solid State Ionics* **2013**, *231*, 109−115.
(10) Chen, R.-J.; Huang, M.; Huang, W.-Z.; Shen, Y.; Lin, Y.-H.; Nan, C.-W. Effect of Calcining and Al Doping on Structure and Conductivity of $Li_7La_3Zr_2O_{12}$. *Solid State Ionics* **2014**, *265*, 7−12.
(11) Geiger, C. A.; Alekseev, E.; Lazic, B.; Fisch, M.; Armbruster, T.; Langner, R.; Fechtelkord, M.; Kim, N.; Pettke, T.; Weppner, W. Crystal Chemistry and Stability of "$Li_7La_3Zr_2O_{12}$" Garnet: A Fast Lithium-Ion Conductor. *Inorg. Chem.* **2011**, *50*, 1089−1097.
(12) Thangadurai, V.; Weppner, W. $Li_6ALa_2Ta_2O_{12}$ (A = Sr, Ba): Novel Garnet-Like Oxides for Fast Lithium Ion Conduction. *Adv. Funct. Mater.* **2005**, *15*, 107−112.
(13) Sudo, R.; Nakata, Y.; Ishiguro, K.; Matsui, M.; Hirano, A.; Takeda, Y.; Yamamoto, O.; Imanishi, N. Interface Behavior between Garnet-Type Lithium-Conducting Solid Electrolyte and Lithium Metal. *Solid State Ionics* **2014**, *262*, 151−154.
(14) Sahu, G.; Rangasamy, E.; Li, J.; Chen, Y.; An, K.; Dudney, N.; Liang, C. A High-Conduction Ge Substituted Li_3AsS_4 Solid Electrolyte with Exceptional Low Activation Energy. *J. Mater. Chem. A* **2014**, *2*, 10396−10403.
(15) Cheng, L.; Crumlin, E. J.; Chen, W.; Qiao, R.; Hou, H.; Franz Lux, S.; Zorba, V.; Russo, R.; Kostecki, R.; Liu, Z.; Persson, K.; Yang, W.; Cabana, J.; Richardson, T.; Chen, G.; Doeff, M. The Origin of High Electrolyte-Electrode Interfacial Resistances in Lithium Cells Containing Garnet Type Solid Electrolytes. *Phys. Chem. Chem. Phys.* **2014**, *16*, 18294−18300.
(16) Cheng, L.; Park, J. S.; Hou, H.; Zorba, V.; Chen, G.; Richardson, T.; Cabana, J.; Russo, R.; Doeff, M. Effect of Microstructure and Surface Impurity Segregation on the Electrical and Electrochemical Properties of Dense Al-Substituted $Li_7La_3Zr_2O_{12}$. *J. Mater. Chem. A* **2014**, *2*, 172−181.
(17) Cheng, L.; Chen, W.; Kunz, M.; Persson, K. A.; Tamura, N.; Chen, G.; Doeff, M. M. Effect of Surface Microstructure on Electrochemical Performance of Garnet Solid Electrolytes. *ACS Appl. Mater. Interfaces* **2015**, *7*, 2073−2081.
(18) Kresse, G. Efficient Iterative Schemes for Ab Initio Total-Energy Calculations Using a Plane-Wave Basis Set. *Phys. Rev. B: Condens. Matter Mater. Phys.* **1996**, *54*, 11169−11186.
(19) Kresse, G.; Joubert, D. From Ultrasoft Pseudopotentials to the Projector Augmented-Wave Method. *Phys. Rev. B: Condens. Matter Mater. Phys.* **1999**, *59*, 1758−1775.
(20) Perdew, J. P.; Burke, K.; Ernzerhof, M. Generalized Gradient Approximation Made Simple. *Phys. Rev. Lett.* **1996**, *77*, 3865−3868.
(21) Jain, A.; Ong, S. P.; Hautier, G.; Chen, W.; Richards, W. D.; Dacek, S.; Cholia, S.; Gunter, D.; Skinner, D.; Ceder, G.; Persson, K. Commentary: The Materials Project: A Materials Genome Approach to Accelerating Materials Innovation. *APL Mater.* **2013**, *1*, 011002.
(22) Awaka, J.; Takashima, A.; Kataoka, K.; Kijima, N.; Idemoto, Y.; Akimoto, J. Crystal Structure of Fast Lithium-Ion-Conducting Cubic $Li_7La_3Zr_2O_{12}$. *Chem. Lett.* **2011**, *40*, 60−62.
(23) Buschmann, H.; Dölle, J.; Berendts, S.; Kuhn, A.; Bottke, P.; Wilkening, M.; Heitjans, P.; Senyshyn, A.; Ehrenberg, H.; Lotnyk, A.; Duppel, V.; Kienle, L.; Janek, J. Structure and Dynamics of the Fast Lithium Ion Conductor "$Li_7La_3Zr_2O_{12}$. *Phys. Chem. Chem. Phys.* **2011**, *13*, 19378−19392.
(24) Persson, K. A.; Waldwick, B.; Lazic, P.; Ceder, G. Prediction of Solid-Aqueous Equilibria: Scheme to Combine First-Principles Calculations of Solids with Experimental Aqueous States. *Phys. Rev. B: Condens. Matter Mater. Phys.* **2012**, *85*, 235438.
(25) Jin, Y.; McGinn, P. J. $Li_7La_3Zr_2O_{12}$ Electrolyte Stability in Air and Fabrication of a $Li/Li_7La_3Zr_2O_{12}/Cu_{0.1}V_2O_5$ Solid-State Battery. *J. Power Sources* **2013**, *239*, 326−331.
(26) Wang, D.; Zhong, G.; Dolotko, O.; Li, Y.; McDonald, M. J.; Mi, J.-X.; Fu, R.; Yang, Y. The Synergistic Effects of Al and Te on the Structure and Li^+ Mobility of the Garnet-Type Solid Electrolytes. *J. Mater. Chem. A* **2014**, *2*, 20271−20279.
(27) Qiao, R.; Chuang, Y.-D.; Yan, S.; Yang, W. Soft X-Ray Irradiation Effects of Li_2O_2, Li_2CO_3 and Li_2O Revealed by Absorption Spectroscopy. *PLoS One* **2012**, *7*, e49182.
(28) Morita, M.; Asai, Y.; Yoshimoto, N.; Ishikawa, M. A Raman Spectroscopic Study of Organic Electrolyte Solutions Based on Binary Solvent Systems of Ethylene Carbonate with Low Viscosity Solvents Which Dissolve Different Lithium Salts. *J. Chem. Soc., Faraday Trans.* **1998**, *94*, 3451−3456.
(29) Downs, R. The RRUFF Project: An Integrated Study of the Chemistry, Crystallography, Raman and Infrared Spectroscopy of Minerals. In *Program and Abstracts of the 19th General Meeting of the International Mineralogical Assoication in Kobe, Janpan*; International Mineralogical Assoication: Bochum, Germany, 2006; pp O03−O13.
(30) Tietz, F.; Wegener, T.; Gerhards, M. T.; Giarola, M.; Mariotto, G. Synthesis and Raman Micro-Spectroscopy Investigation of $Li_7La_3Zr_2O_{12}$. *Solid State Ionics* **2013**, *230*, 77−82.
(31) Larraz, G.; Orera, A.; Sanjuan, M. L. Cubic Phases of Garnet-Type $Li_7La_3Zr_2O_{12}$: The Role of Hydration. *J. Mater. Chem. A* **2013**, *1*, 11419−11428.
(32) Brooker, M. H.; Bates, J. B. Raman and Infrared Spectral Studies of Anhydrous Li_2CO_3 and Na_2CO_3. *J. Chem. Phys.* **1971**, *54*, 4788−4796.
(33) Tanuma, S.; Powell, C. J.; Penn, D. R. Calculations of Electron Inelastic Mean Free Paths. III. Data for 15 Inorganic Compounds over the 50−2000 eV Range. *Surf. Interface Anal.* **1991**, *17*, 927−939.
(34) Rettenwander, D.; Geiger, C. A.; Tribus, M.; Tropper, P.; Amthauer, G. A Synthesis and Crystal Chemical Study of the Fast Ion Conductor $Li_{7-3x}Ga_xLa_3Zr_2O_{12}$ with X = 0.08 to 0.84. *Inorg. Chem.* **2014**, *53*, 6264−6269.
(35) Jin, Y.; McGinn, P. J. Al-Doped $Li_7La_3Zr_2O_{12}$ Synthesized by a Polymerized Complex Method. *J. Power Sources* **2011**, *196*, 8683−8687.
(36) Li, Y.; Wang, Z.; Li, C.; Cao, Y.; Guo, X. Densification and Ionic-Conduction Improvement of Lithium Garnet Solid Electrolytes by Flowing Oxygen Sintering. *J. Power Sources* **2014**, *248*, 642−646.
(37) Li, Y.; Han, J.-T.; Wang, C.-A.; Xie, H.; Goodenough, J. B. Optimizing Li+ Conductivity in a Garnet Framework. *J. Mater. Chem.* **2012**, *22*, 15357−15361.
(38) Ren, Y.; Deng, H.; Chen, R.; Shen, Y.; Lin, Y.; Nan, C.-W. Effects of Li Source on Microstructure and Ionic Conductivity of Al-Contained $Li_{6.75}La_3Zr_{1.75}Ta_{0.25}O_{12}$ Ceramics. *J. Eur. Ceram. Soc.* **2015**, *35*, 561−572.
(39) Buschmann, H.; Berendts, S.; Mogwitz, B.; Janek, J. Lithium Metal Electrode Kinetics and Ionic Conductivity of the Solid Lithium Ion Conductors "$Li_7La_3Zr_2O_{12}$" and $Li_{7-x}La_3Zr_{2-x}Ta_xO_{12}$ with Garnet-Type Structure. *J. Power Sources* **2012**, *206*, 236−244.
(40) Wang, Y.; Lai, W. Phase Transition in Lithium Garnet Oxide Ionic Conductors $Li_7La_3Zr_2O_{12}$: The Role of Ta Substitution and H_2O/CO_2 Exposure. *J. Power Sources* **2015**, *275*, 612−620.
(41) Boryta, D. A.; Maas, A. J. Factors Influencing Rate of Carbon Dioxide Reaction with Lithium Hydroxide. *Ind. Eng. Chem. Process Des. Dev.* **1971**, *10*, 489−494.
(42) Miara, L. J.; Ong, S. P.; Mo, Y.; Richards, W. D.; Park, Y.; Lee, J.-M.; Lee, H. S.; Ceder, G. Effect of Rb and Ta Doping on the Ionic Conductivity and Stability of the Garnet $Li_{7+2x-y}(La_{3-x}Rb_x)(Zr_{2-y}Ta_y)O_{12}$ ($0 \le x \le 0.375$, $0 \le y \le 1$) Superionic Conductor: A First Principles Investigation. *Chem. Mater.* **2013**, *25*, 3048−3055.

DOI: 10.1021/acsami.5b02528
ACS Appl. Mater. Interfaces 2015, 7, 17649−17655